Available online at www.sciencedirect.com

SciVerse ScienceDirect

Ceramics International 39 (2013) 3909–3914

CERAMICS INTERNATIONAL

www.elsevier.com/locate/ceramint

Green gelatine-assisted sol–gel synthesis of ultrasmall nickel oxide nanoparticles

S. Pilban Jahromi[a], N.M. Huang[a,*], M.R. Muhamad[b], H.N. Lim[c]

[a]Low Dimensional Materials Research Centre, Department of Physics, Faculty of Science, University of Malaya, Kuala Lumpur 50603, Malaysia
[b]The Chancellery Building, Multimedia University, Persiaran Multimedia, 63100 Cyberjaya, Selangor Darul Ehsan, Malaysia
[c]Department of Chemistry, Faculty of Science, University Putra Malaysia, 43400 UPM Serdang, Selangor, Malaysia

Received 15 September 2012; received in revised form 20 October 2012; accepted 20 October 2012
Available online 10 November 2012

Abstract

Nickel oxide nanoparticles (NiO NPs) were synthesised using a sol–gel method in a gelatinous medium. Gelatine was used as a size-limiting polymerisation agent for the growth of NiO NPs. X-ray diffraction (XRD) analysis revealed that increasing the calcination temperature increased the crystallite size and decreased the size of the lattice constant. The size-strain plot method (SSP) was used to measure the individual contribution of grain sizes and micro strain on the peak broadening of NiO NPs. Transmission electron microscopy (TEM) showed the ultrasmall size of the NiO NPs with a narrow size distribution(10 ± 0.2 nm). The band gap value of NiO NPs was calculated using ultraviolet–visible (UV–Vis) spectroscopy and decreased with increased calcination temperature.

Keywords: A. Sol–gel; B. Grain size; Nanoparticles; Nickel oxide

1. Introduction

Nanostructured metal oxides exhibit novel properties that are different from those of bulk solid state materials because of the size difference. A reduction in particle size down to the nanoscale level results in various special properties such as quantum size effects, a high specific surface area, and lower sintering temperature [1]. Among metal oxides, NiO nanostructures are p-type semiconductors, with wide band gaps of 3.6–4.0 eV [2]. Furthermore, NiO NPs can be used in various applications, including catalysis [3], battery cathodes [4], electrochromic films [5], fuel cell electrodes, gas sensors [6], photovoltaic devices, and magnetic materials [7]. In addition, NiO NPs are being studied for applications in electrochemical supercapacitors [8], smart windows [9], and dye-sensitised photocathodes [10]. The particle size, shape, and synthesis route of NiO are very important in determining the electrical, optical, and magnetic behaviours of NiO NPs.

Several methods have been developed to synthesise NiO NPs, including sol–gel [11], solvothermal [2], hydrothermal [12], precipitation [13], sonochemical [6], anodic plasma [14], microemulsion [15], and thermal decomposition [16] methods. In general, the preparation of NiO NPs is a complicated process, and a wide variety of different variables may affect the properties of the final products. As we know, there are some essential factors, such as the size, morphology, composition purity, and crystallinity that eventually determine the nanostructure and performance of the final products. Therefore, it is very important to control these factors during the preparation process. The sol–gel synthesis method is one of the simplest and lowest-cost techniques for preparing pure transition metal oxide nanostructures [11]. By selecting an appropriate precursor, products with unique sizes and shapes can be obtained. Organic molecules acting as templates have been used as polymerisation agents to produce nanostructures [17]. Gelatine is one of the green natural polymerisation agents that can be used for these applications [18].

In this work, a simple sol–gel route was adopted to prepare ultrasmall NiO NPs in a gelatine medium [19].

*Corresponding author. Tel.: +60 37 9674295; fax: +60 37 9674146.
E-mail address: huangnayming@um.edu.my (N.M. Huang).

0272-8842/$ - see front matter © 2012 Elsevier Ltd and Techna Group S.r.l. All rights reserved.
http://dx.doi.org/10.1016/j.ceramint.2012.10.237

The calcination temperature was varied to investigate its effect on the crystallinity and optical properties of NiO NPs.

2. Experimental

2.1. Materials

Nickel nitrate was used as the precursor, gelatine was used as the polymerisation agent, and distilled water was used as the solvent. Nickel nitrate ($Ni(NO_3)_2.6H_2O$), was purchased from Acros at a purity of 99%. Gelatine (Type B from bovine skin) was purchased from Sigma Aldrich and was used without further purification.

2.2. Preparation of NiO NPs

To prepare NiO NPs, first 20 g of nickel nitrate ($Ni(NO_3)_2.6\ H_2O$) was dissolved in 40 ml of pure water, then stirred for 40 min. Meanwhile, 10 g of gelatine was dissolved in 150 ml of pure water, then stirred for 30 min at 60 °C to obtain a clear gelatine solution. After that, the nickel nitrate solution was added to the gelatine solution, and the obtained mixed solution was moved to a water bath. The temperature of the water bath was fixed at 80 °C. Stirring was continued for 12 h to obtain a dark green gel. This gel was rubbed on the inner side of a crucible before being left in a furnace at 350 °C for 30 min to achieve the xerogel state. The xerogel was then placed into a horizontal tube furnace (100 cm in length, 5 cm in diameter). High purity O_2 and N_2 gases at a 1:4 volume ratio were fed at about 50 Sccm into the furnace tube at 1 atm of pressure. The furnace was heated from room temperature to 400, 500, 600, and 700 °C at a rate of 10 °C/min. After being held at the final temperature for 1 h, the furnace was cooled down naturally to room temperature.

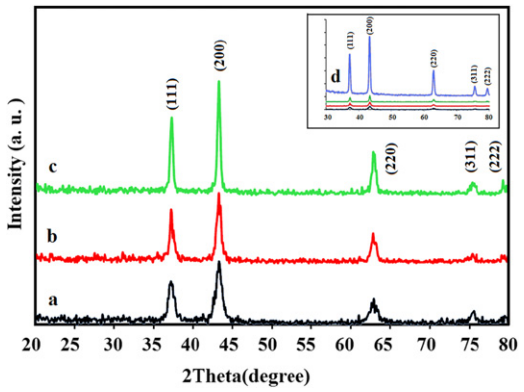

Fig. 1. XRD patterns of NiO NPs after calcination.

2.3. Characterization

The phase purity and crystallite size of the NiO NPs were characterised using XRD (Philips, X'pert, Cu K_α) with a radiation wavelength of $\lambda = 1.54056$ Å, step size 0.1and dwell time 2 s. TEM was carried out on a Hitachi-7100 (acceleration voltage 120 kV) to calculate the average particle sizes of the nanoparticles. The samples were dispersed in ethanol using an ultrasonic bath before placing them onto a copper-coated grid. The UV–Vis (Perkin–Elmer Lambda 750 UV–Vis-NIR spectrophotometer) absorption spectra were recorded in a range of 200–800 nm to determine the band gap energy of the NiO NPs. The samples were dispersed in deionized water.

3. Results and discussion

3.1. X-ray diffraction and crystallite-size analyses

The XRD patterns of the NiO NPs calcined at different temperatures are shown in Fig. 1. All of the XRD patterns clearly show the diffraction peaks of the (1 1 1), (2 0 0), (2 2 0), (3 1 1), and (2 2 2) crystal planes, corresponding to face-centred-cubic (fcc) structured NiO (PDF card No. 01-078-0423). The results show that the synthesised NiO NPs had high purity as there was an absence of impurity peaks. It was observed that the intensity of the diffraction peaks increased as the calcination temperature increased because of the increase in the crystallite size of the NiO NPs. The lattice constants of the prepared samples estimated from the XRD data are presented in Table 1. Several techniques are available to calculate the crystalline size, such as the Scherrer equation ($D = K\lambda/\beta\cos\theta$), in which D is the grain size K is the constant of the Scherrer formula related to index (hkl) and the shape of the NPs, λ is the X-ray wavelength, θ is the XRD diffraction angle, and β is the full width at half maximum (FWHM) of the diffraction peak measured in radians. From the Scherrer equation, parameter β needs to be corrected because the width of the broadening peaks is the result of both the crystalline size and micro-structure strain. In order to correct for β_D, the Gaussian equation is used to separate the effects of the

Table 1
Geometric parameters of NiO NPs calcined at (a) 400 °C, (b) 500 °C, (c) 600 °C, and (d) 700 °C.

Temperature of calcinations (°C)	Average particle size (nm) ± 0.2	Constant lattice (Å)	Size-strain plot D (nm)	Strain	Band gab (eV)
400	10.2	4.181	7.9	0.020	3.91
500	19.2	4.179	13.3	0.006	3.86
600	35.8	4.178	16.0	0.005	3.76
700	48.6	4.174	19.0	0.003	3.63

crystalline size and micro-structure strain, as shown in Eq. (1) [20].

$$\beta_D = \left(\beta^2 - \beta^2_{\text{standard}}\right)^{1/2} \quad (1)$$

The Williamson–Hall plotting method is another technique to separate the crystalline size and micro-structure strain effects. In this technique, we considered that these effects contribute to line broadening, which can be separated using the Lorentzian equation, as shown in Eq. (2).

$$\beta_{\text{hkl}} = \beta_D \pm \beta_\varepsilon \quad (2)$$

where β_D is the width of the diffraction peak caused by the particle size, β_ε is the width of the diffraction caused by the micro-strain, and β is the full line width corrected for instrumental effects. The positive and negative signs indicate lattice expansion and lattice compression, respectively [21]. However, a better evaluation of the size-strain factors in the case of isotropic line broadening can be obtained by considering an average size-strain plot (SSP), which gives less weight to data from reflections at high angles, where the accuracy is usually lower. In this approximation, it is assumed that the crystallite size profile and the strain profile are described by a Lorentzian and a Gaussian function, respectively. The total peak broadening is obtained from Eq. (3).

$$\left(d_{\text{hkl}}\beta_{\text{hkl}}\cos\boldsymbol{\theta}\right)^2 = \frac{A}{D}\left(d^2_{\text{hkl}}\beta_{\text{hkl}}\cos\boldsymbol{\theta}\right) + \left(\frac{\varepsilon}{2}\right)^2 \quad (3)$$

The constant A depends on the shape of the particles [22].

In Fig. 2, the term $\left(d_{\text{hkl}}\beta_{\text{hkl}}\cos\boldsymbol{\theta}\right)^2$ is plotted with respect to $A/D \times \left(d^2_{\text{hkl}}\beta_{\text{hkl}}\cos\boldsymbol{\theta}\right)$ for all of the diffraction peaks of the NiO NPs with the cubic phase from $2\theta = 20^\circ$ to $2\theta = 80^\circ$. In this case, the crystalline size is determined from the slope of the linearly fitted data, where the root of the y-intercept gives the strain. The results obtained from the SSP models are summarised in Table 1. It was clearly seen that the crystallite size of the NiO NPs increased by increasing the calcination temperature. Furthermore, the size of the lattice constant

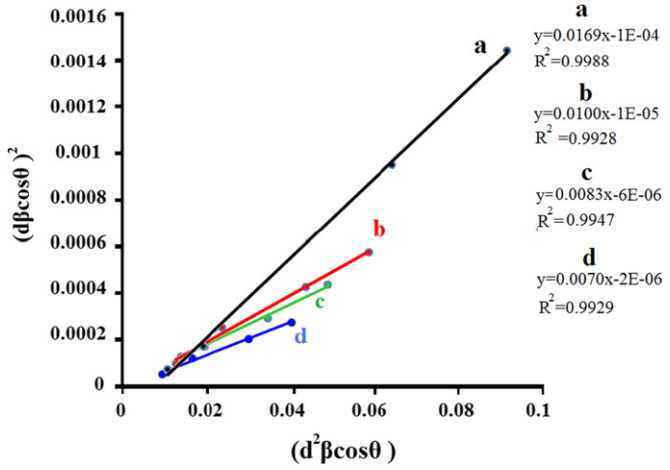

Fig. 2. SSP plot of NiO NPs calcined at (a) 400 °C, (b) 500 °C, (c) 600 °C, and (d) 700 °C. The particle size is determined from the slope of the linearly fitted data while the root of the y-intercept gives the strain.

decreased because of the increase in the size of the particles, which decreased the micro-strain. Although the effect of particle size on the lattice constant has been noted, the reasons for it are ambiguous. Some authors [23] have assumed that it is a consequence of the Laplace pressure, $P = 2\delta/r$, where δ is the surface tension and r is the diameter of the NPs. In addition, the concentration of vacancies might have an effect on the size of the lattice constant [23].

3.2. Morphological studies

The TEM images of the NiO NPs and their corresponding size distribution histograms are given in Fig. 3. According to these size distribution histograms, average particle sizes of 10.2 ± 0.2, 19.2 ± 0.2, 35.8 ± 0.2, and 48.6 ± 0.2 nm were obtained for NiO NPs prepared at calcination temperatures of 400, 500, 600, and 700 °C, respectively. The mean particle size results estimated from the TEM micrographs are in good agreement with the XRD analysis, where the average particle size increased as the calcination temperature increased.

Fig. 4 shows crystallite and particle size as a function of temperature. Particle growth was greater than crystal growth. This shows that the agglomeration of primary NPs (formed at low temperature) plays an important role in the growth of NPs that are calcined at a higher temperature. The NiO samples calcined at 500, 600, and 700 °C showed larger particle sizes with wider size distributions compared to the NiO sample calcined at 400 °C. The coalescence of primary particles in the agglomerates led to the elimination of primary particles below 20 nm in size because of the higher calcination temperature. The small primary particles tended to be connected together. This created larger particles, along with rapidly minimised interfacial free energy, which is proportional to $2\gamma/R$, where R is the radius of spherical particles and is the specific interfacial free energy [24].

3.3. Optical structure

The UV–Vis absorption spectra were investigated in the range of 200–800 nm for NiO NPs synthesised at different calcination temperatures of 400, 500, 600, and 700 °C, (Fig. 5). The absorption coefficient was very low for photon energies in the visible region, while a rapid increase in the absorption coefficient occurred in the UV region. Absorption peaks centred at 318, 320, 323, and 333 nm were observed for the NiO NPs calcined at 400, 500, 600, and 700 °C, respectively, which can be attributed to the intrinsic band gap absorption of NiO NPs. A blue shift was exhibited by the sample calcined at a lower temperature because of the smaller particle size [25].

A common way to obtain the band gap from absorbance spectra is to get the first derivative of the absorbance with respect to the photon energy and find the maximum in the derivative spectrum, as shown in the inset of Fig. 5. The band gaps of the NiO NPs were estimated at about 3.91, 3.86, 3.76, and 3.63 eV for NiO NPs calcined at 400, 500,

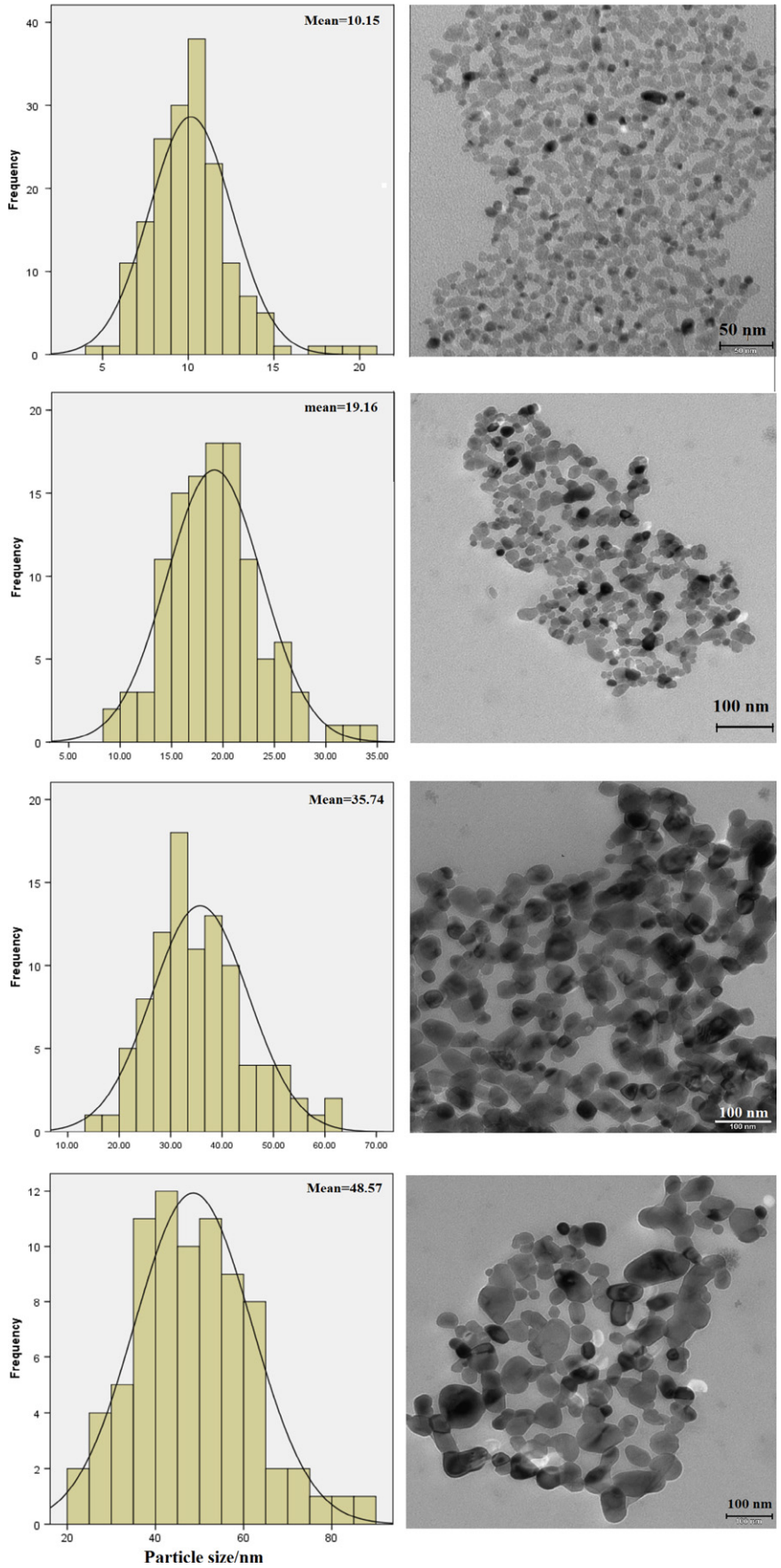

Fig. 3. Size distribution (shown on the left-hand side) and TEM micrographs (shown on the right-hand side) of NiO NPs calcined at (a) 400 °C, (b) 500 °C, (c) 600 °C, and (d) 700 °C.

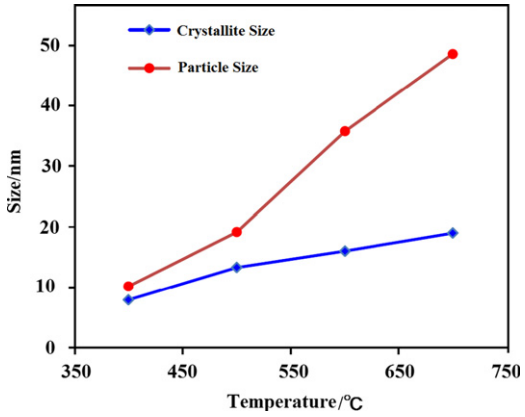

Fig. 4. A profile of crystallite size and particle size versus temperature.

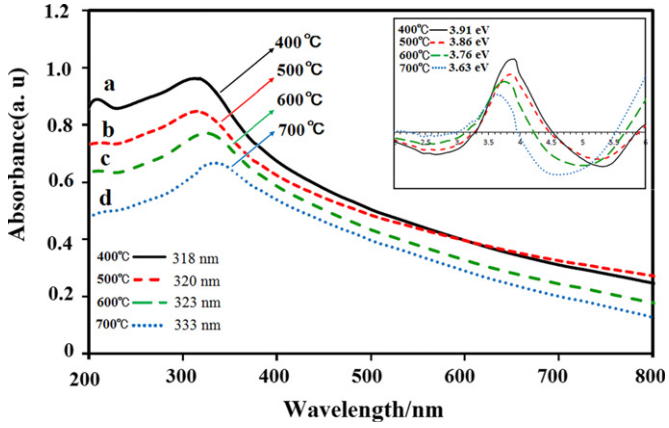

Fig. 5. UV–Vis spectrum of the NiO NPs at (a) 400 °C, (b) 500 °C, (c) 600 °C, and (d) 700 °C. Inset shows the derivative of the absorbance spectrum.

600, and 700 °C, respectively. These estimated band gap energies are in good agreement with the results reported for NiO NPs, which are in the range of 3.6–4.0 eV [2].

4. Conclusion

NiO NPs were prepared by a low cost sol–gel method using gelatine as a green polymerisation agent. During the calcination of the NiO samples, the gelatine acted as a size-limiting agent, producing NiO NPs with very small dimensions and a narrow size distribution. The calcination temperature played an important role in controlling the particle size, with 400 °C found to be the best calcination temperature.

Acknowledgments

This work was financially supported by a High Impact Research Grant (UM.C/625/1/HIR/030) from the University of Malaya and a High Impact Research Grant from the Ministry of Higher Education Malaysia (UM.C/625/1/HIR/MOHE/05). We gratefully acknowledge the University of Malaya for research grant No. PS350-2010B.

References

[1] Y. Wu, Y. He, T. Wu, T. Chen, W. Weng, H. Wan, Influence of some parameters on the synthesis of nanosized NiO material by modified sol–gel method, Materials Letters 61 (14-15) (2007) 3174–3178.
[2] K. Anandan, V. Rajendran, Morphological and size effects of NiO nanoparticles via solvothermal process and their optical properties, Materials Science in Semiconductor Processing 14 (1) (2011) 43–47.
[3] Y. Wang, J. Zhu, X. Yang, L. Lu, X. Wang, Preparation of NiO nanoparticles and their catalytic activity in the thermal decomposition of ammonium perchlorate, Thermochimica Acta 437 (1-2) (2005) 106–109.
[4] M.-S. Wu, Y.-P. Lin, Monodispersed macroporous architecture of nickel-oxide film as an anode material for thin-film lithium-ion batteries, Electrochimica Acta 56 (5) (2011) 2068–2073.
[5] Y.-Z. Zheng, M.-L. Zhang, Preparation and electrochemical properties of nickel oxide by molten-salt synthesis, Materials Letters 61 (18) (2007) 3967–3969.
[6] A. Aslani, V. Oroojpour, M. Fallahi, Sonochemical synthesis, size controlling and gas sensing properties of NiO nanoparticles, Applied Surface Science 257 (9) (2011) 4056–4061.
[7] A.C. Johnston-Peck, J. Wang, J.B. Tracy, Synthesis and structural and magnetic characterization of Ni(Core)/NiO(Shell) nanoparticles, ACS Nano 3 (5) (2009) 1077–1084.
[8] P. Justin, S.K. Meher, G.R. Rao, Tuning of capacitance behavior of NiO using anionic, cationic, and nonionic surfactants by hydrothermal synthesis, Journal of Physical Chemistry C 114 (11) (2010) 5203–5210.
[9] J. Bandara, C.M. Divarathne, S.D. Nanayakkara, Fabrication of n–p junction electrodes made of n-type SnO2 and p-type NiO for control of charge recombination in dye sensitized solar cells, Solar Energy Materials and Solar Cells 81 (4) (2004) 429–437.
[10] X. Wang, J.M. Song, L.S. Gao, J.Y. Jin, H.G. Zheng, Z.D. Zhang, Optical and electrochemical properties of nanosized NiO via thermal decomposition of nickel oxalate nanofibres, Nanotechnology 16 (1) (2005) 37–39.
[11] Q. Li, L.S. Wang, B.Y. Hu, C. Yang, L. Zhou, L. Zhang, Preparation and characterization of NiO nanoparticles through calcination of malate gel, Materials Letters 61 (8-9) (2007) 1615–1618.
[12] M.-G. Ma, J.-F. Zhu, J.-X. Jiang, R.-C. Sun, Hydrothermal–polyol route to synthesis of β-Ni(OH)$_2$ and NiO in mixed solvents of 1, 4-butanediol and water, Materials Letters 63 (21) (2009) 1791–1793.
[13] X. Xin, Z. Lu, B. Zhou, X. Huang, R. Zhu, X. Sha, Y. Zhang, W. Su, Effect of synthesis conditions on the performance of weakly agglomerated nanocrystalline NiO, Journal of Alloys and Compounds 427 (1-2) (2007) 251–255.
[14] H. Qiao, Z. Wei, H. Yang, L. Zhu, X. Yan, Preparation and characterization of NiO nanoparticles by anodic arc plasma method, Journal of Nanomaterials (2009).
[15] T. Ahmad, K.V. Ramanujachary, S.E. Lofland, A.K. Ganguli, Magnetic and electrochemical properties of nickel oxide nanoparticles obtained by the reverse-micellar route, Solid State Sciences 8 (5) (2006) 425–430.
[16] F. Davar, Z. Fereshteh, M. Salavati-Niasari, Nanoparticles Ni and NiO: synthesis, characterization and magnetic properties, Journal of Alloys and Compounds 476 (1-2) (2009) 797–801.
[17] D.G. Shchukin, A.A. Yaremchenko, M.G.S. Ferreira, V.V. Kharton, Polymer gel templating synthesis of nanocrystalline oxide anodes, Chemistry of Materials 17 (20) (2005) 5124–5129.
[18] A.O.G. Maia, C.T. Meneses, A.S. Menezes, W.H. Flores, D.M.A. Melo, J.M. Sasaki, Synthesis and X-ray structural characterization of NiO nanoparticles obtained through gelatin, Journal of Non-Crystalline Solids 352 (32-35) (2006) 3729–3733.
[19] Y. Gan, F. B. Gu, D. M. Han, Z. H. Wang, G. S. Guo, Biomimetic synthesis of zinc oxide 3D architectures with gelatin as matrix, Journal of Nanomaterials (2010) Article ID 289173 (7 pages).

[20] C. Krill, R. Birringer, Estimating grain-size distributions in nanocrystalline materials from X-ray diffraction profile analysis, Philosophical Magazine A77 (1998) 621–626.
[21] N.S. Goncalves, J.A. Carvalho, Z.M. Lima, J.M. Sasaki, Size-strain study of NiO nanoparticles by X-ray powder diffraction line broadening, Materials Letters 72 (2012) 36–38.
[22] I. Lucks, P. Lamparter, E.J. Mittemeijer, An evaluation of methods of diffraction-line broadening analysis applied to ball-milled molybdenum, Journal of Applied Crystallography 37 (2004) 300–305.
[23] A.I. Gusev, A.A. Remple, Nanocrystalline Materials, (2004).
[24] A. Weibel, R. Bouchet, F. Boulc'h, P. Knauth, The big problem of small particles: a comparison of methods for determination of particle size in nanocrystalline anatase powders, Chemistry of Materials 17 (9) (2005) 2378–2385.
[25] B.T. Raut, S.G. Pawar, M.A. Chougule, S. Sen, V.B. Patil, New process for synthesis of nickel oxide thin films and their characterization, Journal of Alloys and Compounds 509 (37) (2011) 9065–9070.